The Astrophysical Journal, 702:480–488, 2009 September 1 doi:10.1088/0004-637X/702/1/480

FORMATION CRITERIA AND THE MASS OF SECONDARY POPULATION III STARS

Hajime Susa[1], Masayuki Umemura[2], and Kenji Hasegawa[2]
[1] Department of Physics, Konan University, Okamoto, Kobe, Japan; susa@konan-u.ac.jp
[2] Center for Computational Sciences, University of Tsukuba, Japan; umemura@ccs.tsukuba.ac.jp, hasegawa@ccs.tsukuba.ac.jp
Received 2009 March 25; accepted 2009 July 16; published 2009 August 12

ABSTRACT

We explore the formation of secondary Population III (Pop III) stars under radiation hydrodynamic (RHD) feedback by a preformed massive star. To properly treat RHD feedback, we perform three-dimensional RHD simulations incorporating the radiative transfer of ionizing photons as well as H_2 dissociating photons from a preformed star. A collapsing gas cloud is settled at a given distance from a 120 $M_\odot$ Pop III star, and the evolution of the cloud is pursued including RHD feedback. We derive the threshold density depending on the distance, above which the cloud can keep collapsing owing to the shielding of H_2 dissociating radiation. We find that an H_2 shell formed ahead of an ionizing front works effectively to shield the H_2 dissociating radiation, leading to the positive feedback for the secondary Pop III star formation. Also, near the threshold density, the envelope of gas cloud is stripped significantly by a shock associated with an ionizing front. By comparing the mass accretion timescale with the Kelvin–Helmholtz timescale, we estimate the mass of secondary Pop III stars. It turns out that the stripping by a shock can reduce the mass of secondary Pop III stars down to $\approx$20 $M_\odot$.

Key words: cosmology: theory – galaxies: formation – hydrodynamics – molecular processes – radiative transfer

Online-only material: color figures

1. INTRODUCTION

The formation of Population III (hereafter Pop III) stars has been explored extensively by many authors (Bromm et al. 1999, 2002; Nakamura & Umemura 1999, 2001; Abel et al. 2000, 2002; Yoshida 2006; Yoshida et al. 2006; O'Shea & Norman 2007), and it is expected that the mass function of Pop III stars is top-heavy with a peak of 100–1000 $M_\odot$. But, the mass range of Pop III stars is not so clear. The enhanced H_2 cooling in pre-ionized gas may reduce the mass (Shapiro & Kang 1987; Susa et al. 1998; Oh & Haiman 2002). If the HD cooling is efficient in fossil H II regions, the mass could be some 10 $M_\odot$ (e.g., Uehara & Inutsuka 2000; Nakamura & Umemura 2002; Nagakura & Omukai 2005; Johnson & Bromm 2006; Greif & Bromm 2006; Yoshida et al. 2007). Also, the variations of cosmological density fluctuations may lead to the formation of less massive Pop III stars with some 10 $M_\odot$ (O'Shea & Norman 2007). However, the radiation hydrodynamic effect on the mass of secondary Pop III stars forming nearby a preformed massive star has not hitherto explored in detail. From an observational point of view, the elemental abundance patterns of hyper-metal-poor stars well match the yields by supernova (SN) explosions with a progenitor mass of $\sim$25 $M_\odot$ (Umeda & Nomoto 2003; Iwamoto et al. 2005). This implies that Pop III stars of some 10 $M_\odot$ are likely to have formed before the first metal enrichment.

Metal-free first objects are expected to collapse at $20 \lesssim z \lesssim 30$, forming a minihalo with a mass of $\approx 10^6$ $M_\odot$ and an extent of $\approx$100 pc (Tegmark et al. 1997; Nishi & Susa 1999; Fuller & Couchman 2000; Yoshida et al. 2003). In the course of bottom-up structure formation, such minihalos merge to form first galaxies at $z \gtrsim 10$, with virial temperature $\gtrsim 10^4$ K and mass $\gtrsim 10^8$ $M_\odot$. Even in the evolution of first galaxies, Pop III stars can play a significant role, since an appreciable number of stars can form from a metal-free component in interstellar gas (Tornatore et al. 2007; Johnson et al. 2008). Also, these Pop III stars are likely to be responsible for the reionization of the universe (Cen 2003; Ciardi et al. 2003; Wyithe & Loeb 2004; Somerville & Livio 2003; Sokasian et al. 2004; Murakami et al. 2005) and the metal enrichment of intergalactic medium (Nakamura & Umemura 2001; Scannapieco et al. 2002; Ricotti & Ostriker 2004) through SN explosions (Mori et al. 2002; Bromm et al. 2003; Kitayama & Yoshida 2005; Greif et al. 2007). Hence, the mass range of Pop III stars affects the galaxy formation and the evolution of intergalactic matter.

If first stars are very massive, they emit intensive ultraviolet (UV) radiation, which significantly influences the subsequent star formation in minihalos or first galaxies (Haiman et al. 1997; Omukai & Nishi 1999; Haiman et al. 2000; Glover & Brand 2001; Machacek et al. 2001). In a Pop III minihalo, primordial fluctuations generate density peaks owing to gravitational instability induced by H_2 cooling. A highest peak collapses earlier to form a first Pop III star as shown by Abel et al. (2002). Subsequently, lower peaks collapse to form cloud cores with a density of 10^2–10^4 cm^{-3} and a temperature of 200–500 K (Bromm et al. 2002). Hence, later collapsing cores could be affected by the radiative feedback by the first star. In first galaxies, the interstellar medium can be pre-ionized by shock, since the virial temperature is higher than 10^4 K. The pre-ionization can promote rapid H_2 formation (Shapiro & Kang 1987; Kang & Shapiro 1992; Susa et al. 1998; Oh & Haiman 2002). As a result, the temperature of interstellar gas in first galaxies can be lowered down to 100 K through efficient H_2 cooling (Johnson et al. 2008). Low temperature collapsing clouds in first galaxies could be subject to the UV feedback by Pop III stars.

If a first star is distant by more than 1 pc, dense clouds are readily self-shielded from the UV radiation (Tajiri & Umemura 1998; Kitayama et al. 2001; Susa & Umemura 2004a, 2004b; Kitayama et al. 2004; Dijkstra et al. 2004; Alvarez et al. 2006). Thus, the photoevaporation by UV heating is unlikely to work devastatingly. However, Lyman–Werner (LW) band radiation (11.18–13.6 eV) photodissociates H_2 molecules, and therefore can preclude a cloud core from collapsing. Hence, the photodissociation of H_2 may lead to momentous negative feedback (Haiman et al. 1997, 2000; Omukai & Nishi 1999;

Glover & Brand 2001; Machacek et al. 2001). Recently, Susa (2007) performed three-dimensional radiation hydrodynamic simulations on the photodissociation feedback, and derived the criteria of the feedback.

However, ionizing radiation ($\geqslant$ 13.6 eV) is related to H_2 formation in an intricate fashion. An ionization front (I-front) driven by ionizing radiation propagates in a collapsing core. The enhanced fraction of electrons catalyzes rapid H_2 formation (Shapiro & Kang 1987; Kang & Shapiro 1992; Susa et al. 1998; Oh & Haiman 2002). In particular, the mild ionization ahead of the I-front can generate an H_2 shell, which potentially shields H_2 dissociating photons (Ricotti et al. 2001). This mechanism is likely to work positively to form Pop III stars. When UV irradiates a dense core, the I-front changes from R-type on the surface to D-type inside the core. The transition occurs via an intermediate type (M-type), which is accompanied with the generation of shock (Kahn 1954). The shock can significantly affect the collapse of the core. This is a totally radiation hydrodynamic (RHD) process. Such radiation hydrodynamic feedback has been investigated by one-dimensional spherical RHD simulations (Ahn & Shapiro 2007), two-dimensional cylindrical RHD simulations (Whalen et al. 2008), and three-dimensional RHD simulations (Susa & Umemura 2006). The results by two-dimensional and three-dimensional simulations are in good agreement with each other. However, quantitative feedback effects, including the compression and stripping by a shock, have not been explored yet over a wide parameter range in three-dimensional simulations.

In this paper, we attempt to investigate quantitatively the RHD feedback on a collapsing cloud by a preformed first star. For this purpose, we solve the three-dimensional RHD in a wide range of parameter space. In the simulations, the radiative transfer of ionizing photons as well as H_2 dissociating photons is self-consistently coupled with smoothed particle hydrodynamics (SPH). In Section 2, the numerical method is described. The setup of simulations is presented in Section 3, and numerical results are given in Section 4. In Section 5, the formation criteria of secondary Pop III stars are numerically derived taking RHD feedback into account. In Section 6, the mass of secondary Pop III stars is estimated. Section 7 is devoted to the conclusions and discussion.

2. NUMERICAL METHOD

We perform numerical simulations with the radiation hydrodynamics code that we developed (Susa 2006). In this section, we briefly summarize the scheme. The code is designed to investigate the formation and evolution of the first-generation objects at $z \gtrsim 10$, where the radiative feedback from various sources plays important roles. The code can compute the fraction of the chemical species e^-, H^+, H, H^-, H_2, and H_2^+ through fully implicit time integration. It can also deal with multiple sources of ionizing radiation as well as the radiation at the LW band. Although there may be heavy elements in first galaxies through Pop III SN explosions therein, the metallic cooling is not dominant as long as the metallicity is lower than $10^{-2}\ Z_\odot$ (Susa & Umemura 2000). In this paper, we ignore the metallic cooling.

The hydrodynamics is calculated by the SPH method. We use the version of SPH by Umemura (1993), with the modification according to Steinmetz & Muller (1993). We adopt the particle resizing formalism by Thacker et al. (2000).

The nonequilibrium chemistry and radiative cooling for primordial gas are calculated with the code developed by Susa & Kitayama (2000), where the H_2 cooling and reaction rates are mostly taken from Galli & Palla (1998). As for the photoionization process, we employ the so-called on-the-spot approximation (Spitzer 1978), where it is assumed that recombination photons to ground states of hydrogen are absorbed promptly on the spot, while recombination photons to excited states can escape the medium. In the present version of our code, we do not take into account helium ionization. For pure hydrogen gas with on-the-spot approximation, we do not need the frequency bins for the radiation field. All we need is the optical depth at Lyman limit, since we know the frequency dependence of the optical depth. We can obtain the "precise" photoionization rate or the photoheating rate as functions of the optical depth at Lyman limit before we start simulations (Susa 2006). We also remark that in case we include helium, we need more frequencies (Nakamoto et al. 2001; Susa 2006).

The optical depth is integrated using the neighbor lists of SPH particles. It is similar to the code described in Susa & Umemura (2004a), but now we can deal with multiple point sources. In our new scheme, we do not create as many grid points on the light ray as the previous code (Susa & Umemura 2004a) does. Instead, we just create one grid point per SPH particle located in its neighbor. We find the "upstream" particle for each SPH particle on its line of sight to the source. Then the optical depth from the source to the SPH particle is obtained by summing up the optical depth at the "upstream" particle and the differential optical depth between the two particles.

The opacity against LW-band flux ($F_{\rm LW}$) is calculated with the self-shielding function by Draine & Bertoldi (1996), which is given by

$$F_{\rm LW} = F_{\rm LW,0} f_{\rm sh}\left(N_{\rm H_2,14}\right), \tag{1}$$

where $F_{\rm LW,0}$ is the incident flux, $N_{\rm H_2,14} = N_{\rm H_2}/10^{14}$ cm^{-2} is the normalized H_2 column density, and

$$f_{\rm sh}(x) = \begin{cases} 1, x \leqslant 1 \\ x^{-3/4}, x > 1 \end{cases}. \tag{2}$$

The column density of H_2 is evaluated by the method described above. We assume the same absorption for the photons within the LW band between 11.26 and 13.6 eV. The use of the self-shielding function ignores the effects of Doppler shifts of LW lines. If the line is shifted more than thermal broadening width, the opacity at the LW band is greatly reduced. In the present calculations, the collapsing gas cloud converges to Larson–Penston-type similarity solutions. Thus, the infall velocity in the envelope of cloud is as large as the sound velocity. Moreover, the velocity around the core is much smaller than the sound velocity. Therefore, we do not include this effect in the present simulations.

The code is already parallelized with the MPI library. The computational domain is divided by the so-called orthogonal recursive bisection method (Dubinski 1996). The parallelization method for the radiation transfer part is similar to that of the multiple wave front method developed by Nakamoto et al. (2001) and Heinemann et al. (2006), but it is changed to fit the SPH scheme. The code is able to handle self-gravity with a Barnes–Hut tree (Barnes & Hut 1986), which is also parallelized. The code is tested for various standard problems (Susa 2006). We also take part in the code comparison project with other radiation hydrodynamics codes (Iliev et al. 2006, 2009), and we find reasonable agreements with each other.

The present simulations are mainly carried out with a novel hybrid computer system in University of Tsukuba, called *FIRST*

simulator, which has been designed to simulate multicomponent self-gravitating radiation hydrodynamic systems with high accuracy (Umemura et al. 2007). The *FIRST* simulator is composed of 256 nodes with dual Xeon processors, and each node possesses a Blade-GRAPE board, that is, the accelerator of gravity calculations. The peak performance is 36.1 Tflop.

3. SETUP OF SIMULATIONS

We use $N = 524,288 (= 2^{19})$ SPH particles to perform radiation hydrodynamic simulations. We suppose a primordial gas cloud undergoing runaway collapse nearby a preformed massive star. Dark matter is neglected in the present calculations, because we are interested in rather dense cores with $n > 10^2$–10^4 cm^{-3} that start to become baryon dominated (e.g., Abel et al. 2002). The tidal field from other halos could have some effects on the dynamics of collapsing gas, which is not taken into account in the present calculation. The chemical compositions are initially assumed to have the cosmological residual value (Galli & Palla 1998). The mass of the cloud is $M_b = 8.3 \times 10^4\, M_\odot$ in a baryonic component. The gas of the cloud is initially at rest and has a "top-hat" density distribution. Initially we also assume uniform temperature. Remark that the density distribution converges to an ordinary $\rho \propto r^{-2}$ profile as the collapse proceeds (e.g., Abel et al. 2002). Also, we distribute a low-density ($n \simeq 10^{-1}$ cm^{-3}) uniform gas around the collapsing cloud. When the central density of the cloud exceeds a certain value, n_{on}, we ignite a $120\, M_\odot$ Pop III star. The luminosity and the effective temperature of the source star are taken from Baraffe et al. (2001). The ionizing photon number per unit time is $\dot{N}_{ion} = 1.3 \times 10^{50}$ s^{-1}, whereas the LW photon number luminosity is $\dot{N}_{LW} = 1.4 \times 10^{49}$ s^{-1}. The source star is located at the distance D from the center of the collapsing cloud.

First, we see fundamental physical processes of radiative feedback using high/low temperature core models. Then we derive the radiation hydrodynamic feedback criteria by changing n_{on} and D. The basic difference between two models is the initial temperature of the clouds. The high initial temperature results in the low temperature core (LTC), while the low initial temperature does in the high temperature core (HTC). In Figure 1, the cloud collapse in the two cases is shown by temperature versus density at the center. In an LTC model, the relatively high initial temperature ($T_{ini} = 350$ K) allows the efficient formation of H_2 molecules and also leads to the relatively slow gravitational contraction. In this model, the ratio between gravitational energy and initial thermal energy $|W|/U \simeq 2$. Consequently, the core temperature goes down quickly to ≈150 K at the density $n_H \approx 100$ cm^{-3}. Since the size of the core is approximately the Jeans length, a smaller core forms in an LTC model. It is worth noting that the density distribution of collapsing gas for $n_H \gtrsim 10^3$ cm^{-3} is close to the one obtained in cosmological simulations including dark matter gravity (O'Shea & Norman 2007; Susa 2007). In an HTC model, the formation of H_2 molecules is not so rapid owing to the lower initial temperature ($T_{ini} = 100$ K). Also, the initial low pressure ($|W|/U \simeq 3$–4) allows the rapid gravitational contraction. Hence, the temperature in a collapsing phase becomes higher, and eventually a larger core forms. The difference in the core size is significant for the radiative feedback.

The basic models investigated in this paper are shown in Table 1. LTC-ION and HTC-ION include both ionizing and LW-band radiation from a $120\, M_\odot$ star respectively for LTC and HTC models, while LTC-LW and HTC-LW include only LW-band radiation respectively for LTC and HTC models. $T_{c,min}$ is the minimum core temperature after the H_2 cooling instability. In these models, $D = 40$ pc and $n_{on} = 10^3$ cm^{-3} are assumed, but D and n_{on} are changed over a wide range to derive the feedback criteria.

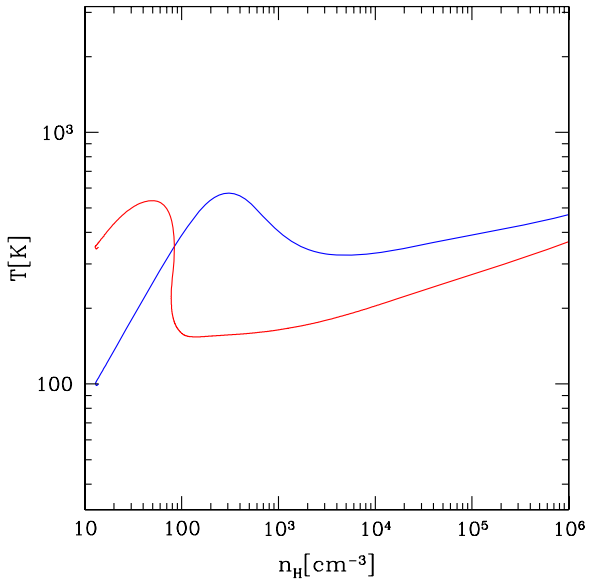

Figure 1. Cloud collapse without radiative feedback. The temperature at the center is shown against the central density for the initial temperatures of 350 K (red curve) and 100 K (blue curve).

(A color version of this figure is available in the online journal.)

Table 1
Basic Models

Model	$T_{c,min}$ (K)	Ionizing Flux	LW band	D (pc)	n_{on} (cm^{-3})
LTC-ION	150	Yes	Yes	40	10^3
LTC-LW	150	No	Yes	40	10^3
HTC-ION	300	Yes	Yes	40	10^3
HTC-LW	300	No	Yes	40	10^3

4. NUMERICAL RESULTS

Here, we see the fundamental physical processes for four basic models shown in Table 1.

4.1. Evolution of Cloud Cores

The time evolutions of cloud cores for four models are shown in Figure 2. In the upper two panels, the temperature and H_2 molecule abundance at the cores are shown against the peak density for LTC-ION and HTC-ION models, while in the lower two panels they are shown for LTC-LW and HTC-LW models.

The cloud evolution is regulated by the formation of H_2 molecule, which is an indispensable coolant for cloud collapse. As seen in Figure 2, the H_2 abundance drops down to a level of 10^{-9} to 10^{-6} immediately by UV radiation after the ignition of a source star (right panels, where the ignition time is marked as 0 Myr). Then, owing to the inefficiency of H_2 cooling, the gravitational contraction becomes adiabatic and temperature rises until 1 Myr (left panels). During the adiabatic contraction, H_2 molecules retrieve, since the H_2 formation rate is raised in adiabatically heated cores.

In the HTC-ION model, the heating by a shock associated with an ionization front helps to increase the temperature. As a result, the H_2 formation is restored and H_2 fraction exceeds $\sim 10^{-4}$. Thus, the core can cool and keep collapsing.

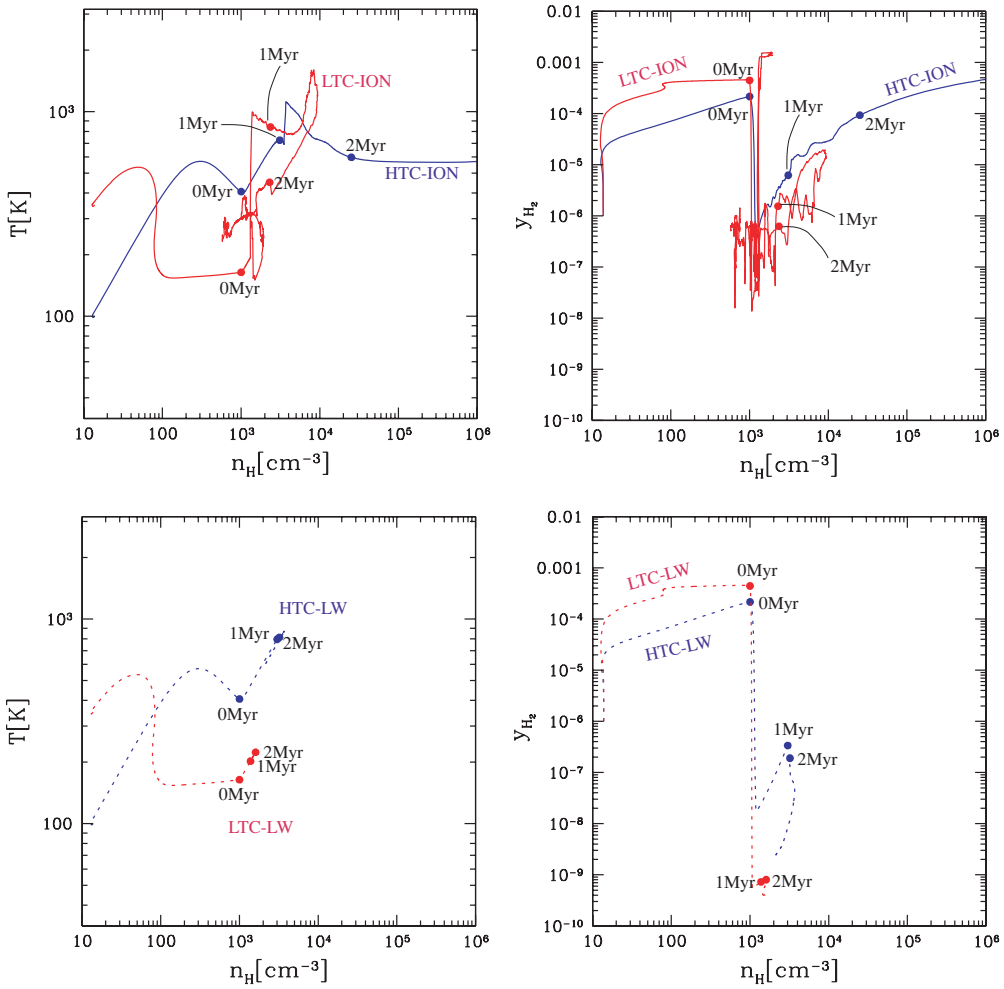

Figure 2. Cloud evolution with radiative feedback for the models listed in Table 1. The time variations of temperature (left two panels) and H_2 molecule abundance (right two panels) at the cores are shown against the peak density. The red solid line depicts LTC-ION model, the blue solid line HTC-ION (upper two panels), the red dotted line LTC-LW, and the blue dotted line HTC-LW (lower two panels). On each curve three stages are indicated by dots, which correspond to 0yr, 1 Myr, and 2 Myr after the ignition of a source star.

(A color version of this figure is available in the online journal.)

In LTC-LW and HTC-LW models, the H_2 abundance drops down to a level lower than 10^{-8} after UV irradiation, and the temperature continues to increase owing to insufficient cooling. Although H_2 formation is recovered, H_2 fractions are not sufficient for the cloud to keep collapsing. Eventually, the cloud core bounces. In the LTC-ION model, the physical processes are more complicated. The shock heating before 1 Myr works importantly to restore H_2 formation. Resultantly, the H_2 abundance reaches to a level of $\sim 10^{-5}$ to 10^{-4}. However, the second hit by a diffracted shock between 1 Myr and 2 Myr (the second peak in a red solid curve in the upper left panel in Figure 2) raises the temperature quickly, so that the core cannot be gravitationally bounded and bounces eventually. Such intricate behavior of a shock is explained further in the following.

4.2. Convergence Check

Ideally, it is appropriate to perform convergence check for all the models; however, we check for the HTC-ION model only, because of the limited computational time. We run three additional simulations with particle numbers $N = 2^{17}$, 2^{18}, and 2^{20}, while the canonical run uses $N = 2^{19}$ particles. Since the highest density peak collapses and we are now interested in the collapse criteria, we plot the evolution of the density peak on the density–temperature plane and the density–H_2 abundance (y_{H_2}) plane for four different resolutions. As shown in Figure 3, all of the results agree fairly well, although the lowest resolution case (long-dashed line) shows some deviation from others. Thus, the resolution of the present simulations are enough to describe the collapse criteria.

4.3. Cloud Structure

The evolution shown above indicates that ionizing radiation works to promote H_2 formation, and therefore help the cloud to collapse. In Figure 4, the spatial distributions of H_2 molecules on the plane including the symmetry axis are shown for LTC-ION and HTC-ION models. Two snapshots are taken at the epoch of 1 Myr and 2 Myr after UV irradiation. Figures 5 and 6 show the gas number density and temperature distributions. Also, we plot various physical quantities along the symmetry axis for all four models in Figure 7.

In the LTC-ION model (the upper two panels in Figures 4–6), the core is self-shielded against ionizing photons and a bow shock forms preceding an ionization front. The bow shock strips the envelope of a collapsing cloud. H_2 molecules are produced efficiently ahead of an ionization front owing to the

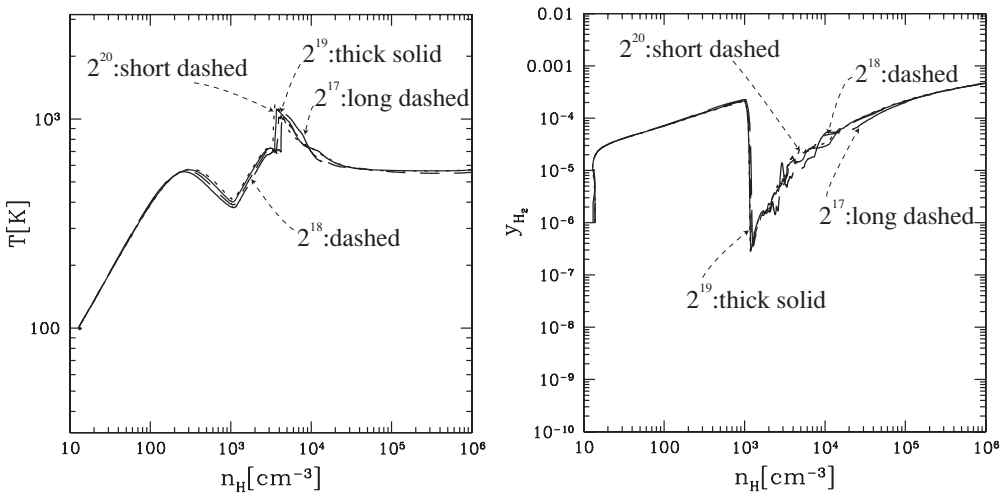

Figure 3. Convergence check on the density–temperature plane (left panel) and the density–H_2 abundance (y_{H_2}) plane for the HTC-ION model. In both the panels, results from four runs are plotted. Short dashed line: $N = 2^{20}$, thick solid line: $N = 2^{19}$ (canonical), dashed line: $N = 2^{18}$, and long dashed line: $N = 2^{17}$.

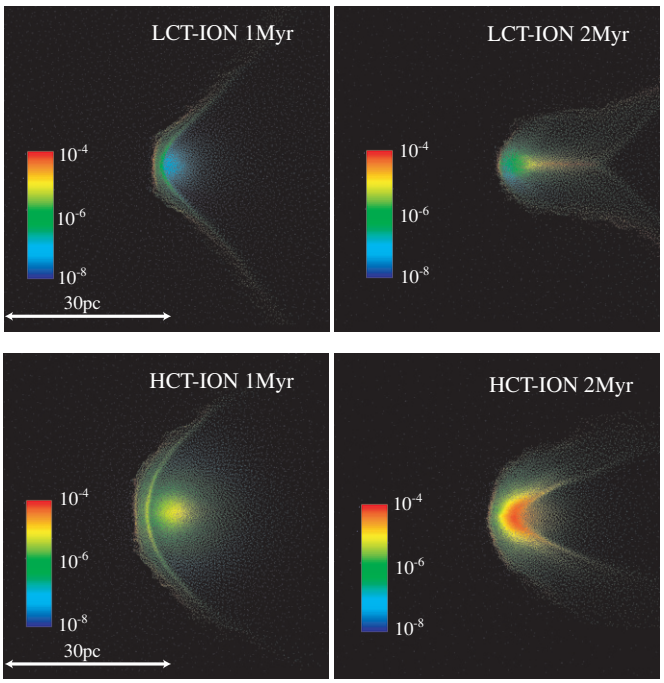

Figure 4. Hydrogen molecule distributions on a plane including the symmetry axis are shown at 1 Myr and 2 Myr after the UV irradiation for HTC-ION and LTC-ION models. The source star is located on the left boundary of each panel. H_2 fractions are shown by colored dots according to the color legend.

(A color version of this figure is available in the online journal.)

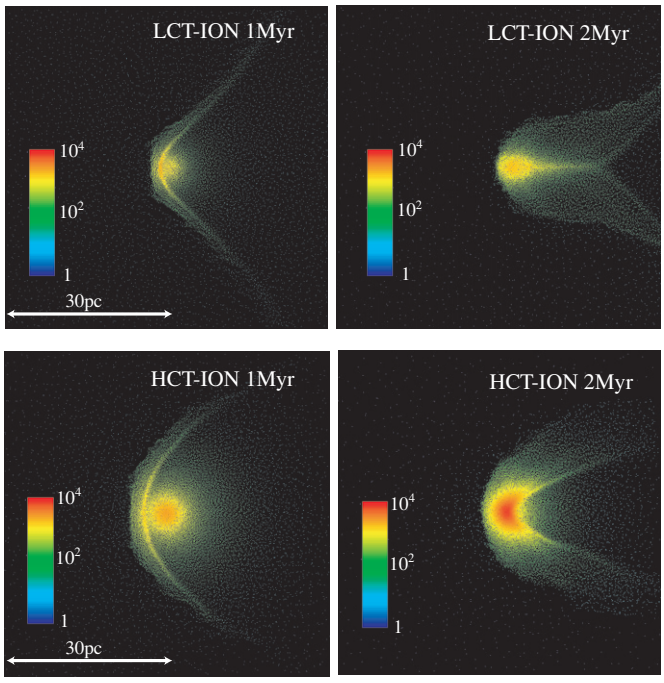

Figure 5. Same as Figure 4, except that the colors of the dots represent the number density of hydrogen nucleus. The color legend is depicted in units of cm^{-3}.

(A color version of this figure is available in the online journal.)

enhanced catalytic effect of free electrons (see also Figure 7). As a result, an H_2 shell is built up and it effectively shields the H_2 dissociating radiation from a source star. In Figure 8, the H_2 column density from the source star is plotted at 1 Myr after UV irradiation. In fact, N_{H_2} at the center of the cloud is several hundred times higher than the critical value 10^{14} cm^{-2} for the shielding of LW-band radiation. Thus, H_2 dissociating radiation is significantly absorbed before it reaches the cloud center. However, as shown in the top-right panel in Figures 4–6, a diffracted shock front hits the cloud core before undergoing the runaway collapse. Consequently, the core bounces owing to the thermal pressure enhanced by the shock. It is also worth noting that we find "an H_2-enriched tail" behind the core. This structure is formed by the collision of shock which is diffracted around the dense core. The temperature of the shock-heated gas is high enough to feed electrons that catalyze the H_2 formation (This structure could be interesting if it fragments into small clumps and yields protostars, although we do not find any sign of such a process in the present simulations. Regarding this issue, higher resolution simulations may be required.).

In the HTC-ION model (the lower two panels in Figures 4–6), a bow shock forms, similar to the LTC-ION model. The H_2 column density at an H_2 shell is comparable to that in the LTC-ION model. However, in this case, the core size is larger than that in the LTC-ION model. Thus, the H_2 column density at the cloud center is roughly 10 times higher than that in the LTC-ION model (see Figure 8). Also, a diffracted shock is not converged into the cloud core before the central density peak goes into a runaway collapse phase. As a result, the cloud core

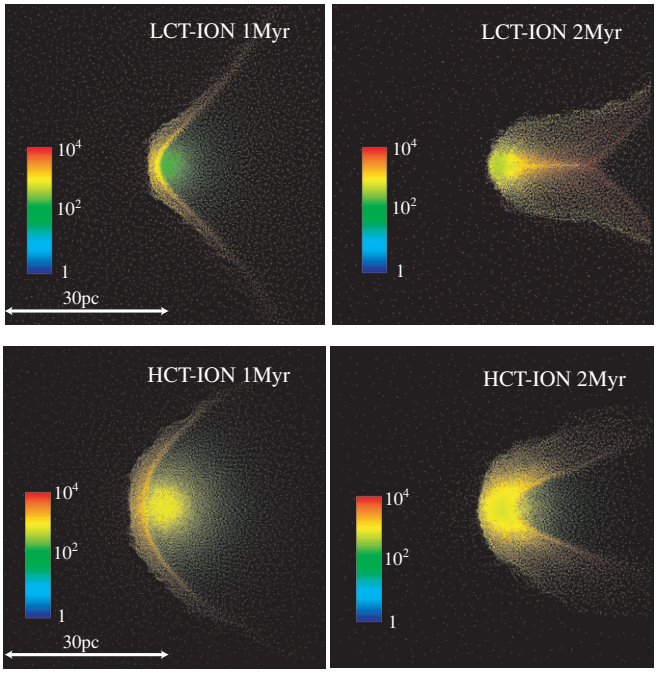

Figure 6. Same as Figure 4, except that the colors of the dots represent the temperature of hydrogen nucleus. The color legend is depicted in units of Kelvin.

(A color version of this figure is available in the online journal.)

can keep collapsing, although the cloud envelope is stripped by a bow shock.

In the LTC-LW model, a smaller core forms owing to its lower temperature. Since the column density of H_2 molecules inside the cloud is low, the self-shielding of H_2 dissociating radiation is very weak (see Figure 7). As a result, the photodissociation of H_2 molecules is so intense to reduce the H_2 abundance to $y_{H_2} \approx 10^{-8}$. Consequently, the cloud core cannot cool and collapse.

In the HTC-LW model, although a large core forms owing to its higher temperature, the dissociating radiation from a source star destructs H_2 molecules to a level of H_2 abundance as $y_{H_2} \approx 10^{-6}$. Hence, the H_2 cooling is not sufficient and the cloud core cannot collapse.

To conclude, within these four models, only the HTC-ION model succeeds in collapsing. The other models result in bouncing after UV irradiation. In other words, the positive feedback overwhelms the negative ones in the HTC-ION model, whereas the negative feedback hinders cloud collapse in LTC-ION, LTC-LW, and HTC-LW models. However, the fate of clouds depends on the distance D from a source star and the core density n_{on} at UV irradiation. Hence, we investigate a wider parameter space to derive the formation criteria of secondary Pop III stars.

5. FORMATION CRITERIA

In addition to the four runs described in the previous section, we perform numerical simulations with various D and n_{on}. Figures 9 and 10 show the results of various runs for LTC and HTC models, respectively. The horizontal axis represents the density n_{on} at turning on a source star and the vertical axis shows the distance D between the source star and the cloud center. In the runs denoted by crosses, the clouds cannot collapse until the end of simulations, i.e., 10^7 years after the ignition of a source star. The open circles represent the runs with successful collapse. These runs can collapse even without ionizing radiation. On the other hand, the runs denoted by open triangles can collapse only if ionizing radiation is present. Here, "a collapsed cloud" is defined as the one whose central density exceeds the numerical resolution limit determined by the Jeans condition. The density corresponding to the resolution limit is $\sim 10^6$–10^7 cm^{-3} in the present simulations. Solid curves show the collapse criterion in the presence of H_2 dissociating radiation only, which is the same as the one obtained by Susa (2007). Figures 9 and 10 show the threshold density depending on the distance, above which the cloud can keep collapsing owing to the shielding of H_2 dissociating radiation.

Interestingly, there is no case where a cloud that can collapse without ionizing radiation fails to collapse by adding ionizing radiation. Near the threshold density, ionizing radiation can rather assist the collapse of a cloud that cannot collapse by H_2 dissociating radiation, as shown by open triangles in Figures 9 and 10. Thus, we can conclude that ionizing flux alleviates the negative feedback by photodissociating radiation to some extent. In LTC models, the parameter region of open triangles is narrower, compared to HTC models. The contrast basically comes from the difference in the core temperature. In both models, the H_2 shell shielding is almost the same, as shown in Figure 8. Also, the mild shock preceding the ionization front heats up the core, which leads to efficient H_2 formation and radiative cooling. This effect is also reported by one-dimensional RHD simulations (Ahn & Shapiro 2007). However, the hydrodynamic evolution in the two models is very different. In HTC models, the central part of the core can cool and collapse with aid of the mild shock heating as well as the H_2 shell shielding. In LTC models, since the core mass and radius are smaller, a diffracted shock front is converged into the core (the upper right panels in Figures 4–6) before the collapse is completed. As a result, the central part of the core is heated up again. This second shock heating is too strong to keep the gas cloud bounded by self-gravity. Thus, the core bounces and evaporates after this second impact by a shock. This negative shock heating mechanism cancels the positive effects by the H_2 shell shielding and mild shock heating in LTC-ION models.

6. MASS OF SECONDARY POP III STARS

To estimate the final stellar mass after the radiation hydrodynamic feedback, the mass accretion timescale is compared to the Kelvin–Helmholtz (KH) contraction timescale, which is adopted from O'Shea & Norman (2007).

Figure 11 shows the mass accretion timescale as a function of enclosed mass from the center of the density peak for several LTC models. The enclosed mass is defined as the mass within a sphere of a given radius. The mass accretion rate $\dot{M}$ is defined as the average of $\dot{M}$ over particles:

$$\dot{M} = \frac{1}{n_{\rm shell}} \sum_{i=1}^{n_{\rm shell}} 4\pi\rho_i \left(\boldsymbol{v}_i - \boldsymbol{v}_{\rm pk}\right) \cdot (\boldsymbol{x}_{\rm pk} - \boldsymbol{x}_i)|\boldsymbol{x}_{\rm pk} - \boldsymbol{x}_i|, \quad (3)$$

where $n_{\rm shell}$ denotes the number of SPH particles within a thin shell $(r, r + \delta r)$, and the summation is taken over the particles within the shell. $\boldsymbol{x}_{\rm pk}$ and $\boldsymbol{v}_{\rm pk}$ denote the position and velocity of the particle at the density peak, and $\boldsymbol{x}_i$ and $\boldsymbol{v}_i$ are those of the particle in the shell.

Five models in which the core collapses successfully are plotted. Four models are LTC models with ionizing photons, while a model denoted by a green curve represents a UV-free

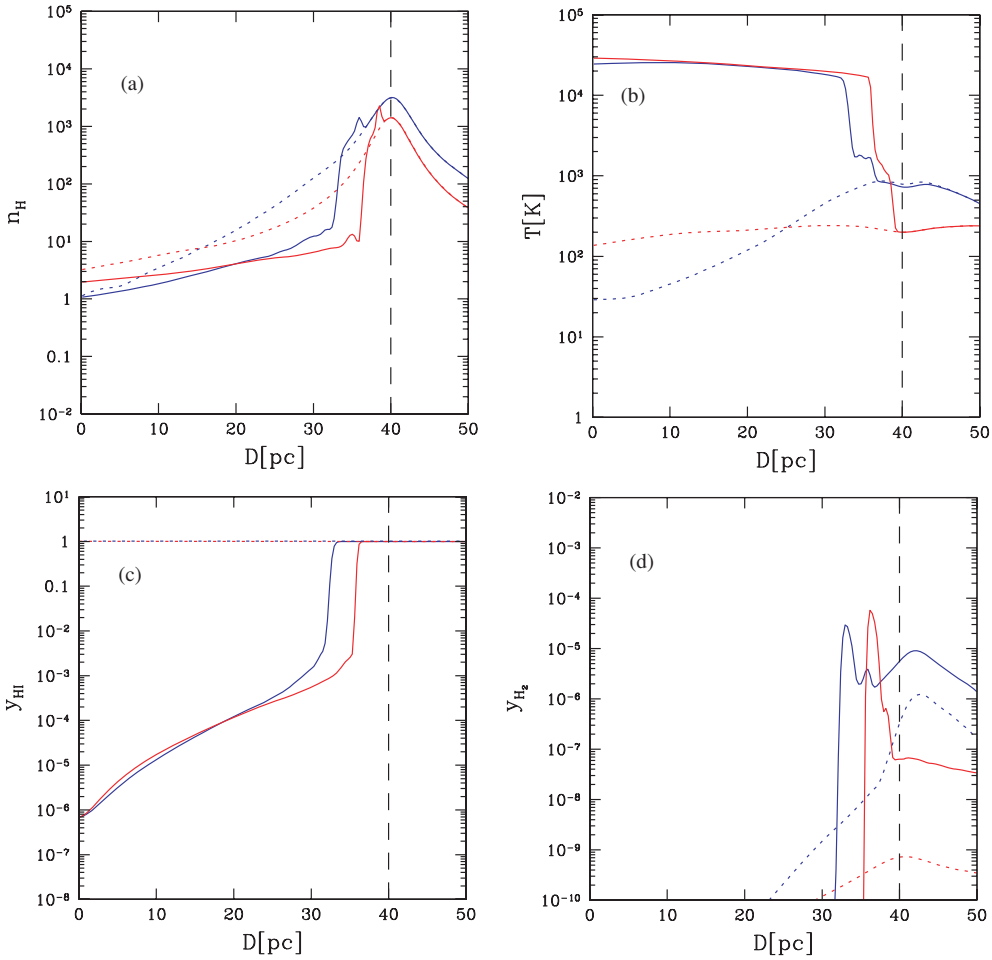

Figure 7. Various physical quantities at 1 Myr after the UV irradiation along the symmetry axis are plotted. Four panels represent (a) hydrogen number density $n_{\rm H}({\rm cm}^{-3})$, (b) temperature T (K), (c) neutral hydrogen abundance $y_{\rm H\,I}$, and (d) H_2 molecule abundance $y_{\rm H_2}$, respectively. The horizontal axis shows the distance from the source star. The blue solid curve depicts the HTC-ION model, the red solid curve LTC-ION, the blue dotted curve HTC-LW, and the red dotted curve LTC-LW. The vertical dashed line in each panel shows the initial position of the cloud center.

(A color version of this figure is available in the online journal.)

(no feedback) case as a reference. In the case of no feedback, the accretion timescale intersects the KH contraction timescale for an enclosed mass of $\sim 6\times10^2\,M_\odot$. This is comparable to the previous estimates (Bromm et al. 1999; Nakamura & Umemura 2001; Abel et al. 2002; Yoshida 2006).

On the other hand, with radiative feedback, the accretion timescale becomes longer than that in no feedback case. For instance, in the model with $n_{\rm on} = 3\times10^3$ cm^{-3} and $D = 100$ pc (blue dotted curve), the mass accreted in the KH timescale is reduced to a level of $\sim 20\,M_\odot$. Therefore, the radiative feedback has a significant impact on the mass of secondary Pop III stars. We also remark that this effect has strong dependence on $n_{\rm on}$ and D. Blue and red dotted curves in Figure 11 denote the model close to the boundary of successful collapse region (see Figure 9), whereas blue and red solid curves correspond to the models slightly distant from the boundary. The mass accretion timescale in latter two models is also prolonged by radiative feedback, but the effect is not so dramatic as the former two models. In these cases, the expected mass of secondary stars is as large as $\approx 100\,M_\odot$.

7. CONCLUSIONS AND DISCUSSION

We have explored the evolution of a collapsing cloud nearby a first luminous star to quantitatively examine radiation hydrodynamic feedback on secondary Pop III star formation. To investigate this issue, three-dimensional radiation SPH simulations have been performed, where the radiative transfer of ionizing photons and H_2 dissociating photons from a first star is self-consistently incorporated. We have derived the numerical criteria for the subsequent Pop III star formation. As a result, we have found that an H_2 shell formed ahead of an ionizing front works effectively to shield the H_2 dissociating radiation, leading to the positive feedback. On the other hand, a shock associated with an ionizing front has a positive effect and a negative effect. The positive one is the compression and heating of gas cloud that promote H_2 formation and thereby accelerate the gravitational instability of the cloud. The negative one is the stripping of gas envelope that reduces the mass accretion rate, leading to the formation of less massive Pop III stars. In a small core, the compression and heating by a shock turns out to be devastating to hinder the cloud collapse. In comparison of the mass accretion timescale with Kelvin–Helmholtz timescale, we have found that the mass of secondary Pop III stars could be reduced to $\approx 20\,M_\odot$.

The possibility that the formation of low-mass Pop III stars with $<100\,M_\odot$ is driven by radiation hydrodynamic feedback would be important in the environment where multiple stars can form within a $\sim(100\ {\rm pc})^3$ volume. In the conventional one-star-per-halo picture, this low-mass star formation mode would

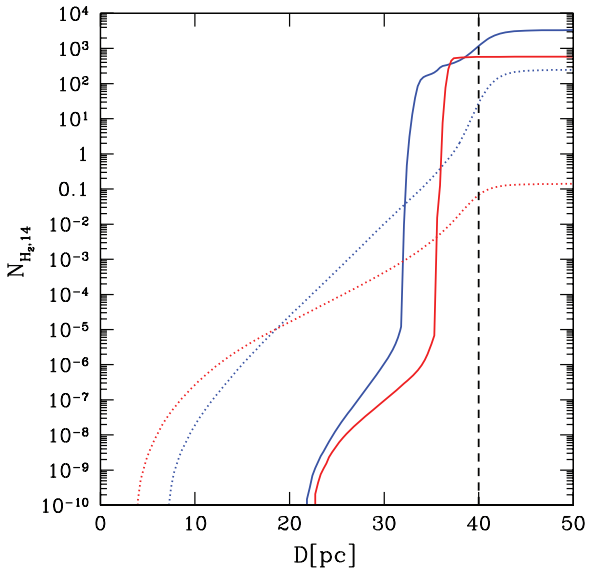

Figure 8. H_2 column density from the source star is shown at 1 Myr after the UV irradiation in units of 10^{14} cm^{-2}. The horizontal axis shows the distance from the source star. The blue solid curve depicts the HTC-ION model, the red solid curve LTC-ION, the blue dotted curve HTC-LW, and the red dotted curve LTC-LW. The vertical dashed line in each panel shows the position of the cloud center.

(A color version of this figure is available in the online journal.)

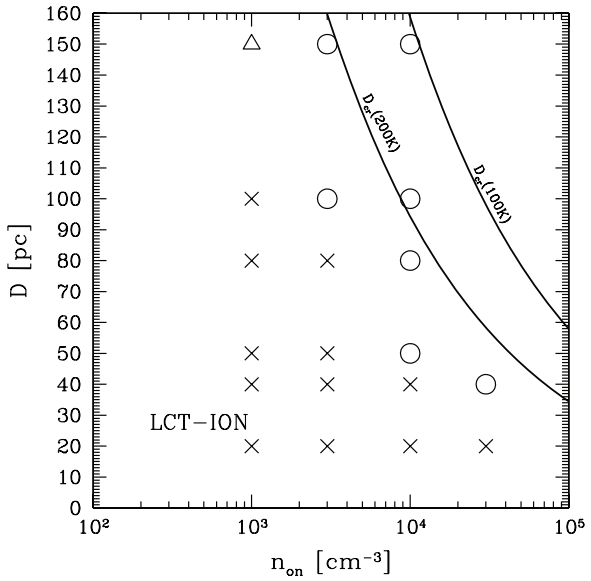

Figure 9. Pop III star formation criteria in LTC models as a function of the central density n_{on} at turning on UV and the distance D from a source star (120 $M_\odot$). Circles succeed in collapsing, while crosses fail to collapse. Triangles also succeed in collapsing, although they fail to collapse in the absence of ionizing photons. Solid curves show the collapse criterion in the presence of H_2 dissociating radiation only (Susa 2007).

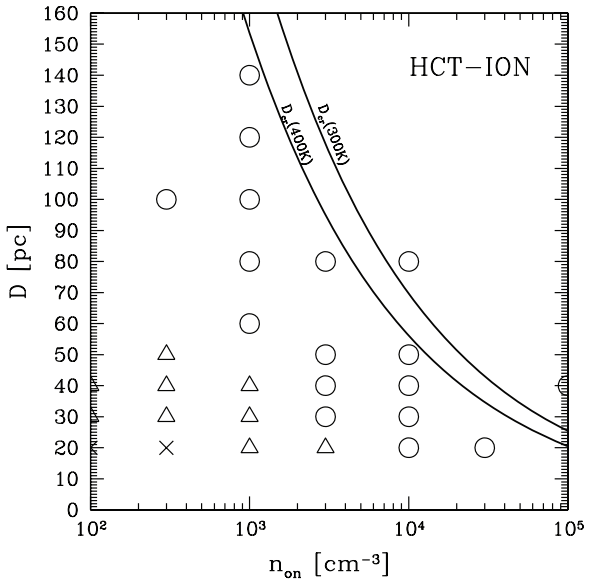

Figure 10. Same as Figure 9, except that the cloud models are HTC models.

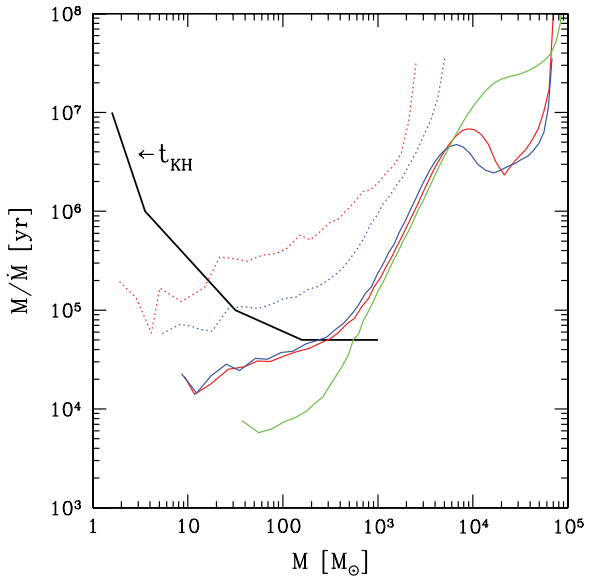

Figure 11. Mass accretion timescale ($M/\dot{M}$) and Kelvin–Helmholtz (KH) contraction timescale are plotted for five models in which the cores successfully collapse. All models are low temperature core models (i.e., $T_{c,min}$ = 150 K). Green line: no feedback, red solid line: $n_{on} = 10^4$ cm^{-3} and D = 100 pc, red dotted line: $n_{on} = 10^4$ cm^{-3} and D = 50 pc, blue solid line: $n_{on} = 3\times10^3$ cm^{-3} and D = 150 pc, and blue dotted: $n_{on} = 3 \times 10^3$ cm^{-3} and D = 100 pc. The black line is the KH contraction timescale adopted from O'Shea & Norman (2007).

(A color version of this figure is available in the online journal.)

not be so important. However, in the case of first galaxies, this mode could play an important role as well as the other modes driven by HD cooling (Uehara & Inutsuka 2000; Nakamura & Umemura 2002; Nagakura & Omukai 2005; Johnson & Bromm 2006; Greif & Bromm 2006; Yoshida et al. 2007). In addition, even in a minihalo, the assumption of one-star-per-halo itself could be modified by resolving dark matter evolution with very high accuracy (M. Umemura et al. 2009, in preparation).

If such lower-mass Pop III stars are formed, the radiation hydrodynamic feedback on further star formation could be changed, since the importance of ionizing radiation relative to H_2 dissociating radiation is different from that of a 120 $M_\odot$ star. Hasegawa et al. (2009) have investigated the dependence on the stellar mass of radiation hydrodynamic feedback and concluded that the ionizing radiation from $\sim$25 $M_\odot$ stars does not have significant impact on the neighboring star formation, but the feedback is essentially determined by H_2 dissociating radiation, which causes only a negative effect.

In the present simulations, we omitted a few processes. First, we do not include the HD chemistry/cooling. It is well known that HD is an important coolant in case once the gas is heated above 10^4 K. In that case, H_2 cooling proceeds faster than the

recombination of hydrogen atom at several thousand Kelvin, leading to a large H_2 fraction, because of "frozen" electrons (Shapiro & Kang 1987; Susa et al. 1998; Oh & Haiman 2002). HD molecules are formed from these abundant H_2 molecules as the collapse of cloud proceeds (e.g., Uehara & Inutsuka 2000; Nakamura & Umemura 2002). Thus, HD cooling could be important when the ionized gas recollapses after the death of the source star. However, in the present simulations, the collapsing density peaks do not experience such a hot phase (Figure 2), because of the self-shielding of the core. The shock associated to the I-front is also too mild to ionize the material (again Figure 2). Thus, as far as the collapse criteria of the core is concerned, HD cooling do not play an important role. Second, we also do not include the H_2–H^+ collision-induced H_2 cooling. According to Glover & Abel (2008), H_2–H^+ collision dominates the excitation of H_2 in case electron fraction $y_e \gtrsim 10^{-2}$ at $T \sim 10^4$ K, and $y_e \gtrsim 10^{-3}$ at $T \sim 10^3$ K. These conditions are marginally satisfied when the gas cools down from ionized state. Thus, H_2–H^+-collision-induced H_2 cooling can play an important role, when the ionized gas recollapses after the source star turned off. However, again in our simulations, it is not so important, since the gas at the density peak is not ionized in its history. It is also worth noting that cooling and dynamics in the neighbor of H_2 shell could be affected by these cooling process (Whalen & Norman 2008), however, it is unlikely that this effect changes the present results.

We thank the anonymous referee for valuable comments. We are grateful to all the collaborators in *Cosmological Radiative Transfer Codes Comparison Project* for fruitful discussions during the three workshops. Numerical simulations have been performed with computational facilities at the Center for Computational Sciences in University of Tsukuba and with computational facilities in Rikkyo University. This work was supported in part by the *FIRST* project based on Grants-in-Aid for Specially Promoted Research by MEXT (16002003) and Grant-in-Aid for Scientific Research (S) by JSPS (20224002) and Inamori Research Foundation.

REFERENCES

Abel, T., Bryan, G. L., & Norman, M. L. 2000, ApJ, 540, 39
Abel, T., Bryan, G. L., & Norman, M. L. 2002, Science, 295, 93
Ahn, K., & Shapiro, P. R. 2007, MNRAS, 375, 881
Alvarez, M. A., Bromm, V., & Shapiro, P. R. 2006, ApJ, 639, 621
Baraffe, I., Heger, A., & Woosely, S. E. 2001, ApJ, 550, 890
Barnes, J., & Hut, P. 1986, Nature, 324, 446
Bromm, V., Coppi, P. S., & Larson, R. B. 1999, ApJ, 527, L5
Bromm, V., Coppi, P. S., & Larson, R. B. 2002, ApJ, 564, 23
Bromm, V., Yoshida, N., & Hernquist, L. 2003, ApJ, 596, L135
Cen, R. 2003, ApJ, 591, L5
Ciardi, B., Ferrara, A., & White, S. D. M. 2003, MNRAS, 344, L7
Dijkstra, M., Haiman, Z., Rees, M. J., & Weinberg, D. H. 2004, ApJ, 601, 666
Draine, B. T., & Bertoldi, F. 1996, ApJ, 468, 269
Dubinski, J. 1996, New Astron., 1, 133
Fuller, T. M., & Couchman, H. M. P. 2000, ApJ, 544, 6
Galli, D., & Palla, F. 1998, A&A, 335, 403
Glover, S. C. O., & Abel, T. 2008, MNRAS, 388, 1627
Glover, S. C. O., & Brand, P. W. J. L. 2001, MNRAS, 321, 385
Greif, T. H., & Bromm, V. 2006, MNRAS, 373, 128
Greif, T. H., Johnson, J. L., Bromm, V., & Klessen, R. S. 2007, ApJ, 670, 1
Haiman, Z., Abel, T., & Rees, M. J. 2000, ApJ, 534, 11
Haiman, Z., Rees, M. J., & Loeb, A. 1997, ApJ, 476, 458
Hasegawa, K., Umemura, M., & Susa, H. 2009, MNRAS, 395, 1280
Heinemann, T., Dobler, W., Nordlund, A., & Brandenburg, A. 2006, A&A, 448, 731
Iliev, I. T., et al. 2006, MNRAS, 371, 1057
Iliev, I. T., et al. 2009, arXiv:0905.2920
Iwamoto, N., Umeda, H., Tominaga, N., Nomoto, K., & Maeda, K. 2005, Science, 309, 451
Johnson, J. L., & Bromm, V. 2006, MNRAS, 366, 247
Johnson, J. L., Greif, T. H., & Bromm, V. 2008, MNRAS, 388, 26
Kahn, F. D. 1954, Bull. Astron. Inst. Neth., 12, 187
Kang, H., & Shapiro, P. 1992, ApJ, 386, 432
Kitayama, T., Susa, H., Umemura, M., & Ikeuchi, S. 2001, MNRAS, 326, 1353
Kitayama, T., & Yoshida, N. 2005, ApJ, 630, 675
Kitayama, T., Yoshida, N., Susa, H., & Umemura, M. 2004, ApJ, 613, 631
Machacek, M. E., Bryan, G. L., & Abel, T. 2001, ApJ, 548, 509
Mori, M., Ferrara, A., & Madau, P. 2002, ApJ, 571, 40
Murakami, T., Yonetoku, D., Umemura, M., Matsubayashi, T., & Yamazaki, R. 2005, ApJ, 625, L13
Nagakura, T., & Omukai, K. 2005, MNRAS, 364, 1378
Nakamoto, T., Umemura, M., & Susa, H. 2001, MNRAS, 321, 593
Nakamura, F., & Umemura, M. 1999, ApJ, 515, 239
Nakamura, F., & Umemura, M. 2001, ApJ, 548, 19
Nakamura, F., & Umemura, M. 2002, ApJ, 569, 549
Nishi, R., & Susa, H. 1999, ApJ, 523, L103
Oh, P., & Haiman, Z. 2002, ApJ, 569, 558
Omukai, K., & Nishi, R. 1999, ApJ, 518, 64
O'Shea, B. W., & Norman, M. L. 2007, ApJ, 654, 66
Ricotti, M., Gnedin, N. Y., & Shull, M. 2001, ApJ, 560, 580
Ricotti, M., & Ostriker, J. P. 2004, MNRAS, 350, 539
Scannapieco, E., Ferrara, A., & Madau, P. 2002, ApJ, 574, 590
Shapiro, P. R., & Kang, H. 1987, ApJ, 318, 32
Sokasian, A., Yoshida, N., Abel, T., Hernquist, L., & Springel, V. 2004, MNRAS, 350, 47
Somerville, R. S., & Livio, M. 2003, ApJ, 593, 611
Spitzer, L., Jr. 1978, Physical Processes in the Interstellar Medium (New York: Wiley)
Steinmetz, M., & Muller, E. 1993, A&A, 268, 391
Susa, H. 2006, PASJ, 58, 445
Susa, H. 2007, ApJ, 659, 908
Susa, H., & Kitayama, T. 2000, MNRAS, 317, 175
Susa, H., Uehara, H., Nishi, R., & Yamada, M. 1998, Prog. Theor. Phys., 100, 63
Susa, H., & Umemura, M. 2000, ApJ, 537, 578
Susa, H., & Umemura, M. 2004a, ApJ, 600, 1
Susa, H., & Umemura, M. 2004b, ApJ, 610, L5
Susa, H., & Umemura, M. 2006, ApJ, 645, L93
Tajiri, Y., & Umemura, M. 1998, ApJ, 502, 59
Tegmark, M., Silk, J., Rees, M. J., Blanchard, A., Abel, T., & Palla, F. 1997, ApJ, 474, 1
Thacker, J., Tittley, R., Pearce, R., Couchman, P., & Thomas, A. 2000, MNRAS, 319, 619
Tornatore, L., Ferrara, A., & Schneider, R. 2007, MNRAS, 382, 945
Uehara, H., & Inutsuka, S. 2000, ApJ, 531, L91
Umeda, H., & Nomoto, K. 2003, Nature, 422, 871
Umemura, M. 1993, ApJ, 406, 361
Umemura, M., Susa, H., Suwa, T., Sato, D., & FIRST Project Team 2007, in AIP Conf. Proc. 990, First Stars III, ed. B. W. O'Shea, A. Heger, & T. Abel (Melville, NY: AIP), 386
Whalen, D., & Norman, M. L. 2008, ApJ, 673, 664
Whalen, D., O'Shea, B. W., Smidt, J., & Norman, M. L. 2008, ApJ, 679, 925
Wyithe, J. S. B., & Loeb, A. 2004, Nature, 427, 815
Yoshida, N. 2006, New Astron. Rev., 50, 19
Yoshida, N., Abel, T., Hernquist, L., & Sugiyama, N. 2003, ApJ, 592, 645
Yoshida, N., Omukai, K., & Hernquist, L. 2007, ApJ, 667, L117
Yoshida, N., Omukai, K., Hernquist, L., & Abel, T. 2006, ApJ, 652, 6